JGR Earth Surface

RESEARCH ARTICLE
10.1029/2025JF008869

# Role of Liquefied Deposition Layers in Modulating Seismic Wave Generation in Surge-Type Debris Flows

**Fengrun Jiang[1,2], Dongri Song[1,2,3,4], Xiaoyu Li[1,2,3], Wei Zhong[1,2,3], Junfeng Li[5], Sunil Poudyal[6], Qi Zhou[7], and Hui Tang[7]**

[1]Key Laboratory of Mountain Hazards and Engineering Resilience/Institute of Mountain Hazards and Environment, Chinese Academy of Sciences, Chengdu, China, [2]University of Chinese Academy of Sciences, Beijing, China, [3]Joint Laboratory of Mountain Hazard Prevention and Mitigation, Institute of Mountain Hazards and Environment, Chinese Academy of Sciences, Chengdu, China, [4]National Cryosphere Desert Data Center, Lanzhou, China, [5]China Institute of Geo-Environment Monitoring, Beijing, China, [6]Department of Civil and Environmental Engineering, Hong Kong University of Science and Technology, Hong Kong SAR, China, [7]GFZ Helmholtz Centre for Geosciences, Potsdam, Germany

**Abstract** Surge-type debris flows propagate as a sequence of surges, forming gradually thickening in situ deposition layers between surges that dynamically alter channel-bed conditions. Seismic recordings from Jiangjia Ravine reveal a progressive attenuation of ground motion amplitude with surge sequence, despite comparable flow magnitudes—indicating a decoupling between flow scale and seismic response. We attribute this to the accumulation and liquefaction of inter-surge deposition layers, rather than pre-existing deposits. To quantify this mechanism, we adopt an effective transmission parameter ($\xi$) within a fluvial seismology-based framework, and propose a sigmoid function linking $\xi$ to normalized deposition layer thickness ($H^*$). This formulation significantly improves the prediction of seismic power spectral density (PSD) across surges and provides a transferable approach to characterize subsurface flow–bed interactions. Our findings underscore the critical role of bed structure evolution during flow in modulating debris-flow-induced seismic signals, with implications for real-time monitoring and early warning in sediment-rich catchments.

**Plain Language Summary** Debris flows are fast-moving hazardous mixtures of water and sediment that travel down mountain channels in a series of surges. As these surges move onto gentle slopes, they leave behind new layers of sediment during motion—called deposition layers. Because the deposition layer can be partially or fully eroded during post-debris-flow flooding, it often leaves minimal physical evidence for subsequent investigations. Our field observations show that these layers, which form within the debris-flow event itself, play a key role in controlling the transmission of seismic waves through the ground. We discovered that as each surge adds more sediment, the ground vibrations become weaker—even when the flows are similar in size. To explain this, we adopted a parameter that describes how the growing deposition layer reduces the effective transmission of seismic signals. We then used this parameter to develop a new model that significantly improves our ability to predict the seismic power spectrum. This provides a novel way to detect hidden changes beneath the surface, especially in remote or hazardous areas where direct measurements are not possible.

**Key Points:**

- Ground vibration decouples from debris-flow magnitude due to the temporary existence of evolving liquefied deposition layers
- A sigmoid function captures the nonlinear relationship between attenuation parameter $\xi$ and normalized deposition layer thickness $H^*$
- Bed structure evolution should be considered in seismic debris-flow monitoring and early-warning systems to improve effectiveness

**Supporting Information:**

Supporting Information may be found in the online version of this article.

**Correspondence to:**

D. Song,
drsong@imde.ac.cn

**Citation:**

Jiang, F., Song, D., Li, X., Zhong, W., Li, J., Poudyal, S., et al. (2026). Role of liquefied deposition layers in modulating seismic wave generation in surge-type debris flows. *Journal of Geophysical Research: Earth Surface*, *131*, e2025JF008869. https://doi.org/10.1029/2025JF008869

Received 12 SEP 2025
Accepted 29 JAN 2026

**Author Contributions:**

**Conceptualization:** Dongri Song
**Data curation:** Fengrun Jiang, Qi Zhou
**Funding acquisition:** Dongri Song
**Methodology:** Fengrun Jiang, Dongri Song
**Supervision:** Dongri Song
**Writing – original draft:** Fengrun Jiang
**Writing – review & editing:** Fengrun Jiang, Dongri Song, Xiaoyu Li, Wei Zhong, Junfeng Li, Sunil Poudyal, Qi Zhou, Hui Tang

© 2026. American Geophysical Union. All Rights Reserved.

## 1. Introduction

Debris flows are unsteady mixtures of water and sediment that commonly propagate as discrete surges rather than continuous flows (Langham et al., 2025). This surge-like behavior has been widely observed across diverse geomorphic settings, such as Jiangjia Ravine in China (Chen et al., 2023), Illgraben in Switzerland (McArdell et al., 2007; Schöffl et al., 2025), Chalk Cliffs in the USA (Coe et al., 2010; Kean et al., 2013), and Gadria Creek in Italy (Schöffl et al., 2023). Surge fronts can attain velocities much higher than trailing flows, leading to intense impacts and high geomorphic and hazard potential (Song et al., 2023).

When debris flows enter lower-gradient channel reaches, they commonly undergo alternating phases of erosion and deposition (Davies, 1986; Edwards et al., 2021; Li et al., 1983). Early surges typically deposit coarse material that builds the basal structure of the bed, which may subsequently develop into stratified paving layers as finer sediment accumulates above (Davies et al., 1992). Later surges generally rework these deposits rather than incise bedrock, producing partial erosion or renewed deposition that modifies flow mobility, runout, and bed structure (Hu et al., 2022; Zhang et al., 2003). Because the bed evolves dynamically, hazard assessments assuming static

basal conditions may underestimate the strength of flow–bed interactions (Chen et al., 2024). Post-event floods can further erode these deposits, often removing evidence of the preceding depositional phases.

These behaviors are consistent with the erosion–deposition wave (EDW) framework developed in granular-flow theory. Laboratory and theoretical studies show that shallow granular flows may organize into waves characterized by cyclic basal arrest and remobilization, with stationary intervals between successive wave crests (Edwards & Gray, 2015; Rocha et al., 2019; Takagi et al., 2011). Recent radar observations provided field-scale evidence of EDWs in natural debris flows (Schöffl et al., 2023), and similar cyclic deposition–reactivation processes have been reported at Jiangjia Ravine (Chen et al., 2024). These findings suggest that surge sequences often contain internal wave dynamics governed by fluctuations in basal stress, pore-fluid pressure, and granular rearrangement, which manifest in the field not only as cyclic arrest–remobilization behavior but also as the progressive formation and evolution of basal deposition layers (Marchi et al., 2002; Viroulet et al., 2019; Zanuttigh & Lamberti, 2007).

Despite the relevance of EDWs for flow mechanics, their influence on seismic energy transmission is not well constrained. How cyclic deposition, consolidation, and reactivation of basal layers affect the attenuation of high-frequency seismic waves remains poorly understood, even though seismic monitoring is increasingly used for debris-flow detection and early-warning applications. Addressing this knowledge gap requires relating the seismic signatures of individual surges to the internal structural transitions occurring at the flow–bed interface. Recent advances in debris-flow monitoring, including seismic arrays, in-channel LiDAR, and ultrasonic flow sensors, have provided new opportunities to resolve debris-flow mechanics with high temporal fidelity (Aaron et al., 2023; Berger et al., 2011; McCoy et al., 2012; Nagl et al., 2020). In particular, seismic monitoring has shifted from simple event detection (Jiang et al., 2023; Li et al., 2020, 2022; Song et al., 2025a; Zhou et al., 2024) to more mechanistic interpretations of signal properties.

Seismic amplitude, frequency, and energy content are increasingly linked to flow dynamics, including frontal impact, bulk transport, flow rheology, and bed interactions (Bachelet et al., 2018; Lai et al., 2018; Tsai et al., 2012). Theoretical models suggest that seismic power spectral density (PSD) scales with momentum transfer at the particle–bed interface, modulated by factors such as flow velocity, grain size, and bed roughness (Lai et al., 2018; Tsai et al., 2012). These insights have enabled a transition from empirical classifications to physics-informed interpretations of debris-flow seismicity.

Experimental studies have demonstrated that elastic waves generated by particle impacts on erodible beds are sensitive to the bed's structure and saturation state. Specifically, thicker or more saturated substrates tend to absorb more energy, reducing the amplitude and clarity of the seismic signal (Bachelet et al., 2018). For example, Kean et al. (2015) showed that static pre-deposited layers attenuate ground motion via viscous damping and disrupted force transmission. However, these experiments treat the bed as static, whereas surge-type debris flows rapidly generate and rework inter-surge deposits; the role of such surge-dependent bed changes in modulating seismic transmission remains unresolved.

Field observations from Jiangjia Ravine point to this gap. During a well-recorded debris-flow sequence in 2010, a bedrock-mounted accelerometer registered high-amplitude signals during the initial surges; however, subsequent —and in some cases larger—surges produced markedly weaker ground motion. This apparent decoupling between surge magnitude and seismic amplitude lacked a mechanistic explanation at the time, in part because the evolution of the near-bed layer was not independently constrained.

In this study, we revisit this phenomenon with a new data set collected during a debris-flow event in Jiangjia Ravine in July 2024. We hypothesize that inter-surge deposition layers evolve into a liquefied, energy-absorbing medium that dampens seismic wave transmission. Thus, the observed reduction in seismic amplitude across successive surges does not necessarily indicate reduced flow energy but rather reflects progressive changes in the subsurface structure. We test this hypothesis using synchronous seismic, video, and flow depth data, and propose a new attenuation parameter $\xi$ to characterize the seismic transmission efficiency as a function of deposition layer development.

## 2. Study Site and Observations

Jiangjia Ravine, located in Yunnan Province, China, is a tributary of the Xiaojiang River—an upper branch of the Yangtze River—renowned for its frequent and high-magnitude debris flows (Figure 1a). Field observations were

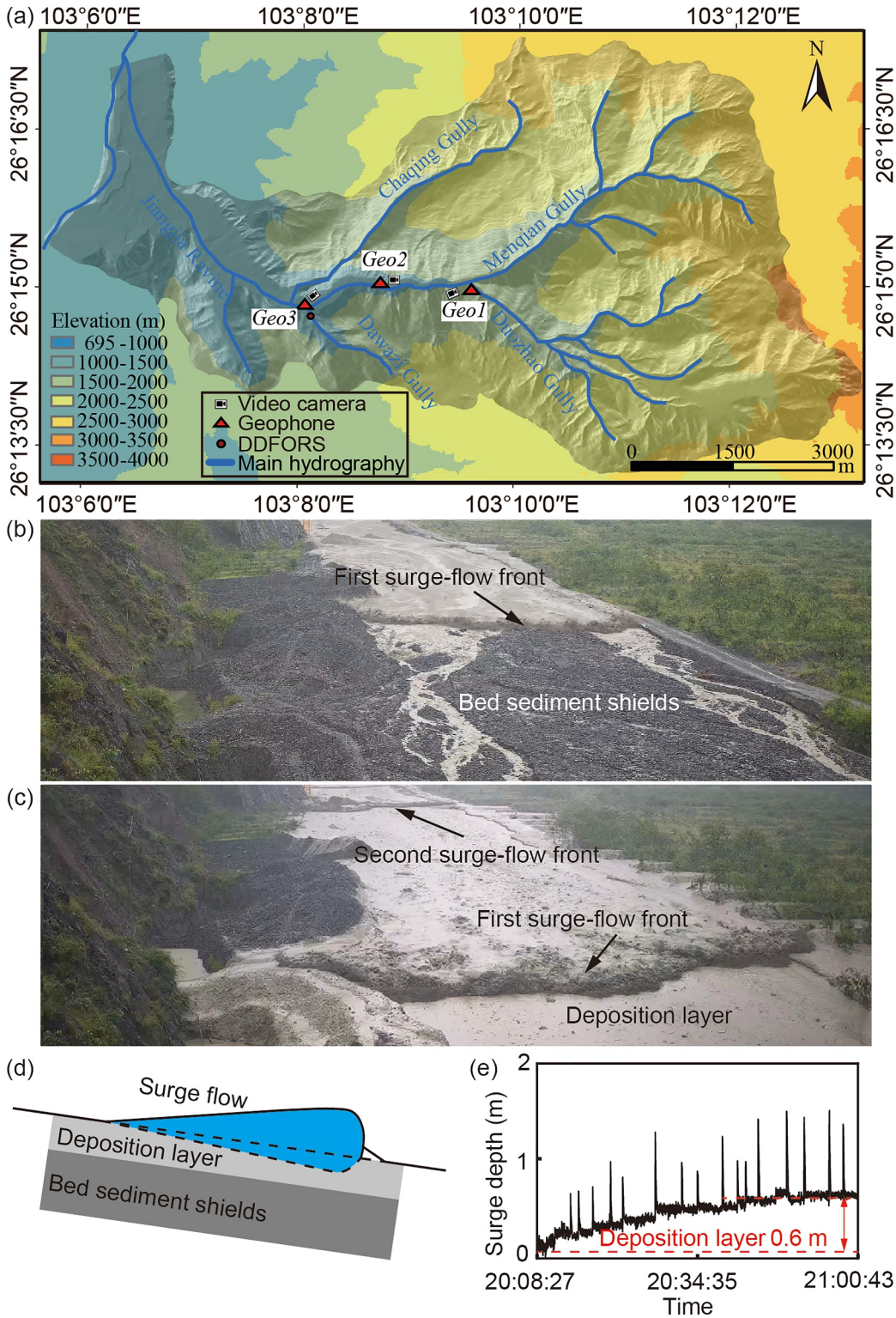


**Figure 1.** Study area and debris flow observations. (a) Plan view of Jiangjia Ravine. Field monitoring setup at DDFORS. (b) Field image of an early surge traveling over a freshly scoured bed with no deposition layer. (c) Field image of a later surge overriding accumulated deposition. (d) Schematic illustration of surge-induced erosion and deposition process. (e) Measured hydrograph showing deposition layer buildup during a debris flow on 24 July 2001.

conducted at the Dongchuan Debris Flow Observation and Research Station (DDFORS), which provides a long-term hydrological and geophysical monitoring infrastructure (Wei et al., 2025). The debris flows in this region are characteristically dense, highly viscous, and composed of multiple surges, making Jiangjia an ideal natural laboratory for investigating the erosion and deposition dynamics and seismic responses of surge-type flows.

To capture the temporal evolution of individual surges and associated bed responses, we deployed an integrated monitoring system comprising triaxial geophones (frequency range: 4.5–100 Hz; 24-bit resolution), video cameras operating at 10 frames per second. This setup enabled synchronous acquisition of seismic waveforms, video imagery, and hydrodynamic parameters during debris flow events. It should be noted that the ultrasonic flow-depth sensor experienced a malfunction during the 28 July 2024 event, preventing the acquisition of a continuous flow-depth time series. Nevertheless, peak frontal flow-depth measurements were successfully obtained for each debris-flow surge, providing reliable constraints on the surge-scale flow depth.

As illustrated in Figures 1b and 1c, the debris flows at Jiangjia typically consist of discrete steep-fronted surges. An event in 2000 demonstrated the full sequence of surge dynamics, including the formation of a basal "pavement" from remnant sediments deposited by late-stage surges (Figure 1d). Figure 1e further highlights the initial surge propagating over a coarse bed surface, followed by progressive sediment accumulation into a saturated basal layer approximately 0.6 m thick.

In this study, we analyzed a debris flow event that occurred on 28 July 2024, which was captured in full by our monitoring system. The flow initiated at 03:24 UTC (11:24 local time) and lasted approximately 1 hr, with surge dynamics recorded on video (Song et al., 2025c). The study reach at Geo3 (Figure 1a) is a straight, constant-slope section of the channel (3.7°) instrumented with seismic (Figure 6b), providing conditions suitable for controlled comparisons of surge behavior. A total of 33 discrete surges and several short continuous-flow intervals were identified from field observations and video analysis (Table 1). Based on their timing and flow behavior, the 28 July 2024 event can be divided into two dynamically distinct phases. Group 1 (Flowing on a stiff bed, Surges 1–17) represents the early phase in which the surges mobilized over a relatively stiff and undeformed basal surface, producing continuous or semi-continuous surge trains. Group 2 (Stationary remobilization, Surges 18–33) corresponds to the later stage, where discrete surges were separated by pronounced inter-surge deposition. These deposits facilitated temporary basal arrest followed by remobilization.

This frequency range was determined from both our spectral analysis (which shows debris-flow energy concentrated within 8–35 Hz, Figure S1 in Supporting Information S1) and previous studies that identified similar frequency bands for debris-flow signals (Belli et al., 2022; Zhou, Cui, et al., 2025; Zhou, Tang, et al., 2025). Applying the same 5–45 Hz filter to all surges ensures consistent comparison of seismic energy attenuation among events. Power Spectral Densities (PSDs) were derived from 100 Hz seismic records using the Welch method with 1024-sample Hanning windows and 50% overlap. Each waveform was de-trended, de-meaned, and zero-phase band-pass filtered (5–45 Hz; narrow transition near 45–50 Hz) to suppress background and sensor noise. Surge windows were manually defined by synchronizing video and seismic data; an analysis window of ∼10 s immediately preceding head arrival was used for PSD computation. All power spectral densities *(PSDs) analyzed in this study are computed from ground velocity records.* Fourier amplitudes were squared, averaged, and normalized to obtain PSDs in $(m/s)^2/Hz$ (or equivalent velocity units), which were then log-scaled (dB) for comparison among surges (Figure 2b).

To systematically assess this phenomenon, we selected three additional surge pairs (Figures 3–5), each carefully controlled for velocity while allowing the surge scale and bed conditions to vary. In each case, the earlier surge traveled over a relatively bare or compact bed, while the later surge propagated over a progressively thickened saturated deposition layer formed by preceding surges. Ground velocity time series and corresponding PSD curves were extracted from the vertical component (Z) recorded by geophone Geo3. To assess whether the progressive buildup of basal sediments attenuates ground vibrations, we focused particularly on Group 2 surges, where the influence of remnant deposition layers on seismic transmission is expected to be most pronounced.

Across all comparisons, the earlier surges generated higher seismic amplitudes and energy, even when smaller in thickness or width. For example, Figure 3 illustrates that Surge 12 (0.4 m thick, 17 m wide, 8.3 m $s^{-1}$) produced stronger ground motion than the later Surge 26 (0.6 m thick, 28 m wide, 8.3 m $s^{-1}$). Similarly, Figure 4 shows that Surge 14 (0.4 m thick, 26 m wide, 7.1 m $s^{-1}$) generated greater seismic output than the larger Surge 27 (0.6 m thick, 28 m wide, 7.1 m $s^{-1}$). In the final comparison (Figure 5), Surge 17 (0.4 m thick, 8 m wide, 4.5 m $s^{-1}$)

**Table 1**
*Flow Width, Flow Height, Front Velocity, and Bulk Density Measured During the 28 July 2024 Debris-Flow Event at Jiangjia Ravine (UTC)*

| Label | Time for surge front $T_1$/(h:m:s) | Surface width $B$/m | Surge front height $h$/m | Front velocity of surge flow $v$/(m/s) | Unit weight $\gamma_c$/(1000 kg/m$^3$) |
|---|---|---|---|---|---|
| 1 | 3:24:52 | 12 | 0.3 | 6.3 | 2.0 |
| 2 | 3:25:28 | 22 | 0.3 | 6.3 | 2.0 |
| 3 | 3:26:04 | 27 | 0.3 | 8.3 | 2.0 |
| 4 | 3:26:24 | 28 | 0.5 | 10.0 | 2.0 |
| 5 | 3:26:53 | 28 | 0.7 | 8.3 | 2.1 |
| 6 | 3:27:17 | 28 | 0.8 | 8.3 | 2.1 |
| 7 | 3:27:40 | 28 | 1.0 | 8.3 | 2.0 |
| 8 | 3:28:05 | 28 | 1.0 | 7.1 | 2.1 |
| 9 | 3:28:34 | 28 | 1.0 | 8.3 | 2.1 |
| 10 | 3:28:52 | 12 | 0.3 | 8.3 | 2.1 |
| C | 3:29:02 | 20 | 0.3 | 8.0 | 2.0 |
| C | 3:29:42 | 15 | 0.3 | 8.0 | 2.0 |
| 11 | 3:30:50 | 27 | 0.6 | 7.1 | 2.1 |
| C | 3:31:14 | 8 | 0.3 | 7.0 | 2.0 |
| 12 | 3:32:17 | 17 | 0.4 | 8.3 | 2.0 |
| C | 3:32:42 | 8 | 0.3 | 8.3 | 2.0 |
| 13 | 3:34:00 | 20 | 0.4 | 10.0 | 1.9 |
| C | 3:34:29 | 8 | 0.3 | 7.1 | 1.9 |
| 14 | 3:35:08 | 26 | 0.4 | 7.1 | 1.9 |
| C | 3:35:21 | 8 | 0.3 | 8.3 | 1.9 |
| 15 | 3:35:51 | 16 | 0.4 | 6.3 | 2.0 |
| C | 3:36:49 | 5 | 0.3 | 8.3 | 1.9 |
| 16 | 3:37:21 | 28 | 0.8 | 8.3 | 2.0 |
| 17 | 3:38:35 | 8 | 0.4 | 4.5 | 1.8 |
| 18 | 3:39:02 | 10 | 0.4 | 5.6 | 1.8 |
| 19 | 3:39:32 | 28 | 0.9 | 7.1 | 2.1 |
| 20 | 3:40:37 | 10 | 0.5 | 6.3 | 2.1 |
| 21 | 3:41:05 | 28 | 0.7 | 7.1 | 2.1 |
| 22 | 3:41:34 | 28 | 0.7 | 10.0 | 2.1 |
| 23 | 3:42:24 | 10 | 0.3 | 5.6 | 1.8 |
| 24 | 3:42:59 | 8 | 0.3 | 4.5 | 1.8 |
| 25 | 3:43:58 | 28 | 0.9 | 8.3 | 2.1 |
| 26 | 3:44:24 | 28 | 0.6 | 8.3 | 2.1 |
| 27 | 3:44:55 | 28 | 0.6 | 7.1 | 2.0 |
| 28 | 3:46:32 | 28 | 0.6 | 4.2 | 2.0 |
| 29 | 3:47:34 | 28 | 0.5 | 4.2 | 1.9 |
| 30 | 3:49:13 | 25 | 0.5 | 4.2 | 1.8 |
| 31 | 3:49:26 | 25 | 0.4 | 2.8 | 1.8 |
| 32 | 3:50:40 | 25 | 0.5 | 4.5 | 1.8 |
| 33 | 3:52:47 | 25 | 0.4 | 4.2 | 1.8 |

*Note.* Surges flow is numbered (1–33), while continuous-flow intervals are labeled "C." All values are derived from field observations and video interpretation.

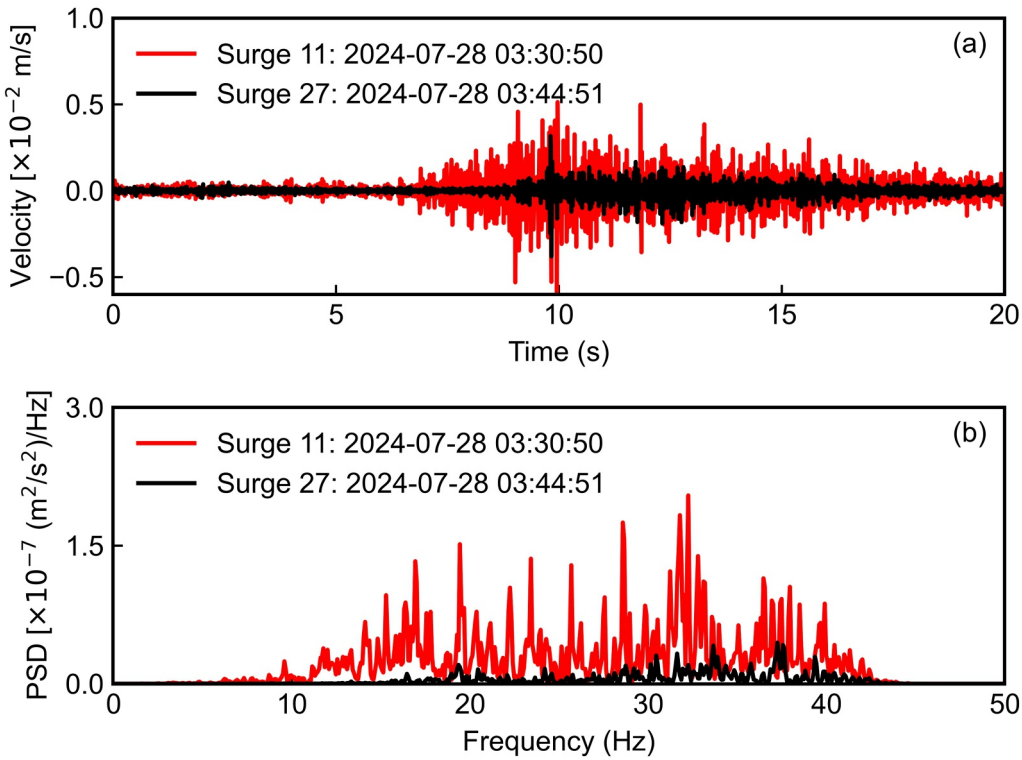


**Figure 2.** Seismic comparison between two representative debris flow surges. (a) Triaxial ground velocity waveforms recorded by geophone Geo3 during Surge 11 (03:30:50 UTC) and Surge 27 (03:44:51 UTC). All waveforms were preprocessed by removing the mean, linear detrending, and applying a band-pass filter between 5 and 45 Hz to isolate the dominant frequency range of debris-flow-induced ground motion. (b) Corresponding power spectral density (PSD) curves derived from the vertical component (Z) of ground motion. Despite Surge 27 being larger in flow width and depth, Surge 11 generated significantly stronger seismic energy across the entire spectrum, illustrating the influence of evolving bed conditions on seismic wave transmission.

produced stronger high-frequency energy than Surge 27 (0.5 m thick, 28 m wide, 4.5 m $s^{-1}$), with peak PSD power concentrated in the 30–40 Hz band.

To quantitatively evaluate the degree of liquefaction of the basal layer, we estimated the liquefaction ratio (LR = $P/\sigma$) following Chen et al. (2023). The calculated LR values of 0.88–0.89 for the 28 July 2024 surges indicate that the pore-fluid pressure approached the total normal stress, suggesting a nearly liquefied state. This provides mechanical evidence that the basal deposition layer behaved as a liquefied medium, consistent with the observed seismic attenuation pattern.

Together, these results provide robust field evidence that the evolving state of the channel bed—notably, the buildup of liquefied inter-surge sediment—plays a dominant role in modulating seismic signal strength. The consistent attenuation observed in later surges supports the hypothesis that subsurface softening and energy dissipation within the deposition layer substantially reduce ground motion, even when flow conditions at the surface appear equally or more energetic.

This counterintuitive result suggests that seismic energy transmission is not solely governed by the instantaneous flow characteristics of a given surge but is also influenced by evolving subsurface conditions—specifically, the progressive accumulation of remnant deposition layers from preceding surges. These deposition layers likely reduce bed stiffness and disrupt seismic coupling efficiency, leading to stronger attenuation of ground vibrations in later surges. As such, these comparative observations provide solid support for our hypothesis that the surge size–seismic amplitude relationship is modulated by the cumulative mechanical effects of subsurface evolution.

We interpret this apparent paradox as evidence of attenuation caused by a progressively thickening and liquefied basal layer. Figure 6 illustrates the hypothesized mechanism: the initial surge traversed a relatively rigid pre-event

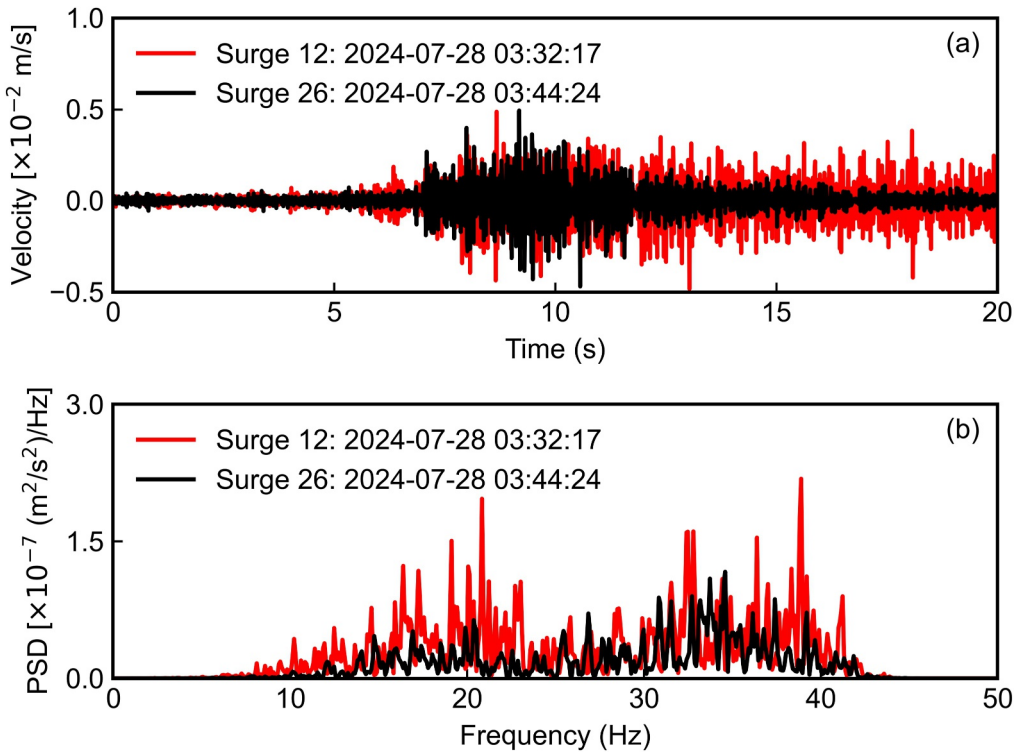


**Figure 3.** Seismic comparison between two representative debris flow surges. (a) Time history of vertical ground velocity recorded by geophone Geo3 during Surge 12 (03:32:17 UTC; red) and Surge 26 (03:44:24 UTC; black). Although Surge 26 was larger in physical dimensions (0.6 m thick, 28 m wide, 8.3 m/s) compared to Surge 12 (0.4 m thick, 17 m wide, 8.3 m/s), it generated a weaker seismic response. (b) Power spectral density (PSD) curves derived from the vertical component show that both surges share a similar dominant frequency range (10–40 Hz), but the earlier smaller surge (Surge 12) exhibits markedly higher spectral power across the band. This highlights enhanced seismic coupling and reduced attenuation in the absence of thick deposition layers.

bed, enabling efficient seismic transmission. In contrast, subsequent surges encountered a liquefied evolving layer that absorbed and scattered seismic energy. This attenuation likely arises from disruption of grain-scale force chains, viscous damping within water-filled pore spaces, and enhanced scattering due to increased heterogeneity of the medium.

## 3. Methods

To test our hypothesis, we employed two complementary theoretical formulations that evaluate the influence of deposition layers on seismic response during surge-type debris flows. These formulations relate debris-flow dynamics to seismic signal characteristics and allow us to quantify the modulation of seismic energy transmission by evolving channel-bed conditions.

### 3.1. Kinetic–Seismic Energy Scaling

The motion of a debris flow can be viewed as a transformation of the gravitational potential energy of the mobilized mass into kinetic energy and ultimately into dissipated forms such as basal friction, fluid–particle interactions, and ground vibrations. In this framework, the debris flow is treated as an integrated mass, and the total energy released during its downslope motion directly governs the strength of the associated seismic signals. Part of this release is dissipated internally within the flow, but a significant fraction is transferred to the channel bed through particle impacts, generating elastic waves that propagate as seismic energy. Consequently, the amplitude and frequency content of the seismic signal provide a measure of how efficiently the flow's bulk energy is coupled into the ground. At the end of motion, when deposition occurs, the remaining kinetic energy vanishes, and the total seismic radiation recorded along the flow path reflects the overall loss of potential energy of the debris mass.

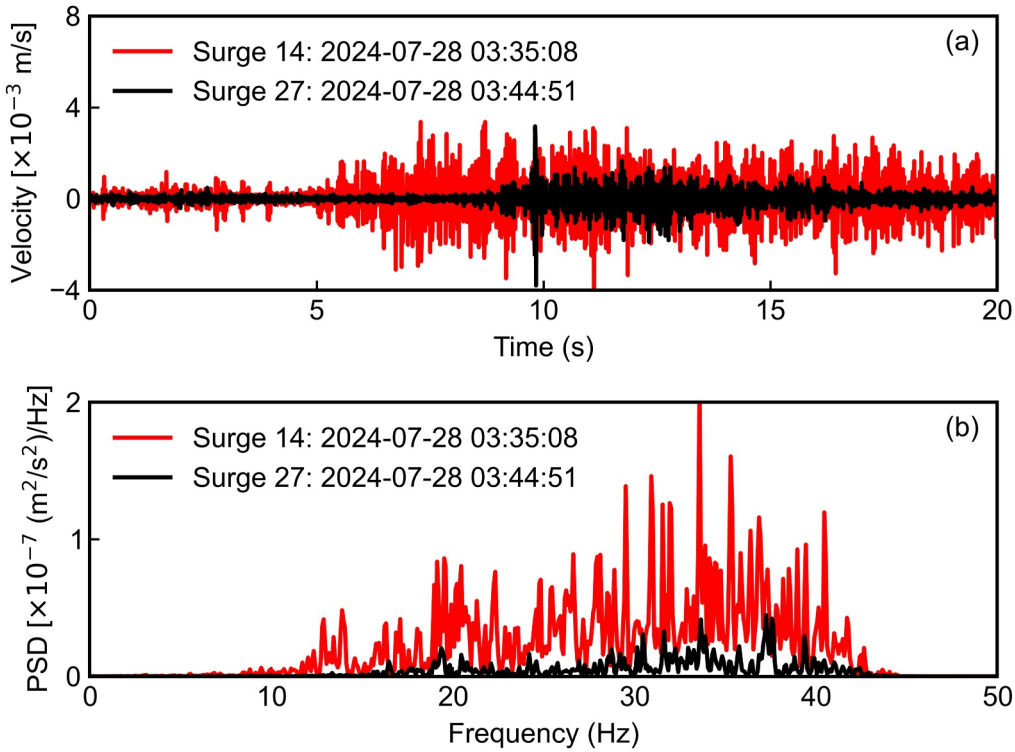


**Figure 4.** Seismic comparison between two representative debris flow surges. (a) Vertical ground velocity time series recorded by geophone Geo3 during Surge 14 (03:35:08 UTC; red) and Surge 27 (03:44:51 UTC; black). Despite being smaller in scale (0.4 m thick, 26 m wide, 7.1 m/s), Surge 14 produced a significantly stronger seismic response than the larger Surge 27 (0.6 m thick, 28 m wide, 7.1 m/s), highlighting a disruption in the typical amplitude–scale relationship. (b) Power spectral density (PSD) analysis reveals similar dominant frequency bands (10–40 Hz) for both surges, yet the earlier smaller surge exhibits substantially higher spectral power. These results point to enhanced seismic coupling in the absence of basal damping layers and support the hypothesis of attenuation caused by progressive subsurface deposition during the debris-flow sequence.

Following Coviello et al. (2019), we assume that the seismic energy radiated by a debris flow surge is linearly proportional to its kinetic energy. This assumption is consistent with earlier work linking granular flow dynamics to seismic emissions (Deparis et al., 2008; Hibert et al., 2011; Levy et al., 2015), wherein solid particle impacts at the bed surface act as the primary energy transfer mechanism. For a given cross-section, the kinetic energy per unit area $E_k$ (J/m$^2$) of a surge front is expressed as:

$$E_k = \frac{1}{2} \cdot m \cdot v^2 \tag{1}$$

where $v$ (m/s) is the surge front velocity, and $m = \rho h$ (kg/m$^2$) is the mass per unit area, with $\rho$ the bulk density (kg/m$^3$) and $h$ the surge height ($m$) relative to the deposition surface. Assuming a scaling between kinetic and seismic energy following Coviello et al. (2019), we test whether the peak amplitude recorded by a near-channel geophone can serve as a proxy for the kinetic energy of the debris-flow front, using field data from the Jiangjia Ravine.

### 3.2. Physics-Based PSD Modeling and Inversion of Seismic Attenuation

To complement the PSD-based analysis, we adopt the physics-based model of Lai et al. (2018), originally developed for seismic radiation from fluvial sediment transport. In this formulation, the vertical ground velocity is expressed as the superposition of surface waves generated by individual particle–bed impacts, and the corresponding power spectral density (PSD) of the ground motion is derived directly from the theoretical treatment of each particle impact on the channel bed:

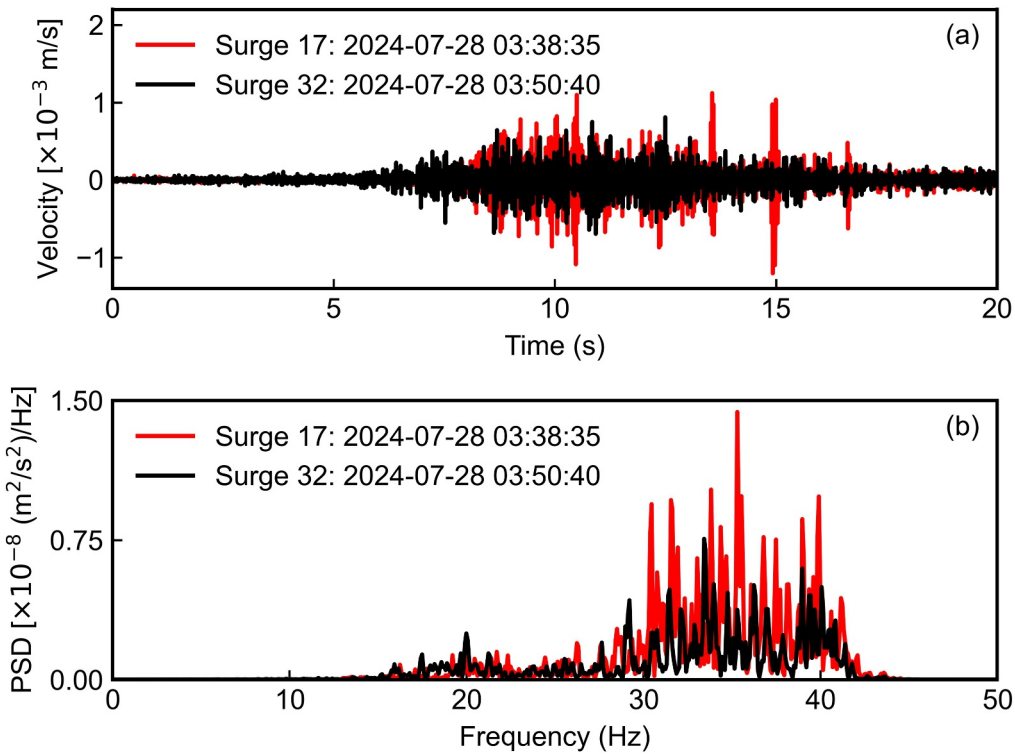


**Figure 5.** Seismic comparison between two representative debris flow surges. (a) Vertical ground velocity time series recorded by geophone Geo3 during Surge 17 (03:38:35 UTC; red) and Surge 27 (03:50:40 UTC; black). Although Surge 17 is smaller in scale (0.4 m thick, 8 m wide, 4.5 m/s), it produces a much stronger seismic response than the larger Surge 27 (0.5 m thick, 28 m wide, 4.5 m/s), suggesting anomalous signal transmission behavior. (b) Power spectral density (PSD) analysis reveals that both surges share a dominant frequency band around 30–40 Hz; however, the earlier smaller surge exhibits significantly greater power. This further demonstrates enhanced seismic coupling prior to substantial bed deposition and highlights the attenuation effect of evolving subsurface layers in surge-type debris flows.

$$\mathcal{P} = \frac{0.6^2(1+\xi)^2\pi^4\rho_D^2}{36\rho_g^2 v_c^5 r_0} \cdot \mathrm{LWD}^3 u^3 \cdot f^{3+5\xi} \cdot e^{-2\pi f^{1+\xi} r_0 (1+\xi)/v_c Q} \tag{2}$$

where, $\mathcal{P}$ represents estimated seismic power spectral density ((m/s)$^2$/Hz). Here, $\xi$ is the velocity-structure parameter introduced by Tsai et al. (2012) that controls the frequency dependence of Rayleigh-wave phase velocity and, consequently, the frequency-dependent attenuation term in the PSD formulation. $\rho_g$ is the bulk ground density (kg/m$^3$), and $\rho_D$ is the density of the debris flow (kg/m$^3$). $v_c$ denotes the Rayleigh wave phase velocity at 1 Hz (m/s), and $Q$ is the Rayleigh wave quality factor, assumed to be frequency-independent within the observed range (Tsai et al., 2012). The frequency $f$ is in hertz. $r_0$ represents the average distance (m) between the seismic station and the debris flow source. $D$ is the 94th percentile of the grain size distribution (m), while $u$ is the mean flow velocity (m/s). $L$ and $W$ denote the length of the boulder-rich snout and the width of the debris flow (m), respectively.

If $\mathrm{L} \gg r_0$, the effective source length is truncated to $\mathrm{L} = r_0$ to account for geometric spreading in seismic wave propagation (Lai et al., 2018). This model allows surge-to-surge inference of changes in effective high-frequency transmission associated with the near-surface structure through $\xi$, which is later estimated for each surge using a surge-by-surge inversion based on the observed PSD.

To quantify the mechanical attenuation induced by evolving bed conditions during surge-type debris flows, we estimate the attenuation parameter $\xi$ for each individual surge using the theoretical framework proposed by Lai et al. (2018). Here $\xi$ is treated as an effective transmission parameter that summarizes surge-to-surge changes in the near-surface structure affecting high-frequency spectral decay in the adopted PSD formulation. We do not interpret $\xi$ as an intrinsic dissipation parameter (i.e., it is distinct from Q), but as a descriptor of the evolving near-

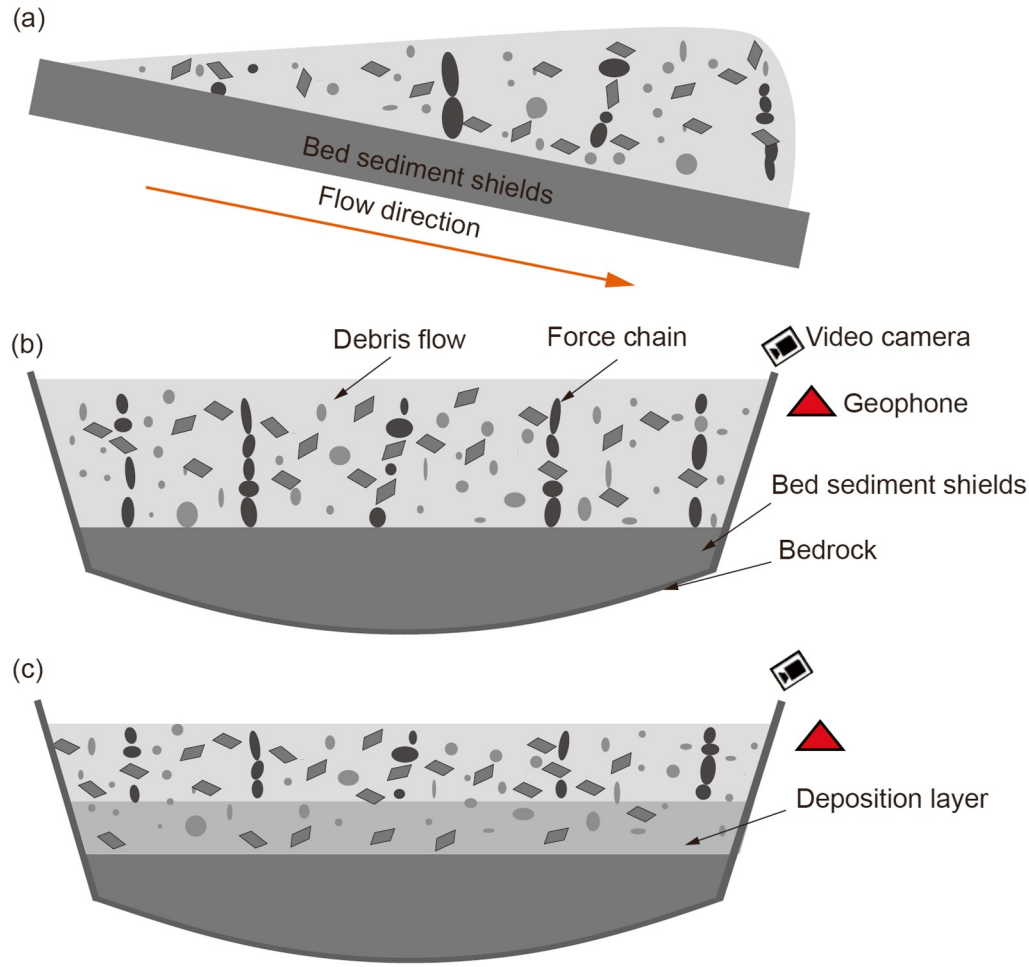


**Figure 6.** Conceptual model of flow–bed interaction during surge-type debris flows. (a) Profile view showing seismic wave propagation during early surges on bed sediment shields. (b) Cross-sectional view of the surge front during the early stage without deposition layer, showing sensors positioned along the channel margin and a strong seismic–flow correlation due to minimal bed accumulation. (c) Surge traveling over a liquefied deposition layer, where progressive subsurface buildup disrupted force chains within the saturated substrate, leading to significant attenuation of seismic-wave transmission.

surface velocity gradient and scattering/impedance structure that modulates the frequency-dependent attenuation term.

For each subsequent surge $i$, the observed seismic power spectral density (PSD), denoted as $P_i$, is normalized against that of the baseline surge $P_0$, resulting in a dimensionless ratio $P_i/P_0$.

This observed ratio is then compared to the theoretical prediction derived from the right-hand side of the following expression (Equation 2), which models seismic attenuation as a function of $\xi$:

$$\mathcal{P}(\xi) \propto f^{3+5\xi} \cdot e^{-2\pi f^{1+\xi} r_0 (1+\xi)/v_c Q} \tag{3}$$

In seismological theory, the parameter $\xi$ describes the frequency dependence of Rayleigh-wave phase velocity and reflects the vertical velocity gradient of the near-surface medium (Tsai et al., 2012), rather than intrinsic energy dissipation. In our PSD formulation, $\xi$ enters both the power-law factor $f^{3+5\xi}$ and the exponential attenuation factor $\exp\{-2\pi f^{1+\xi} r_0 (1+\xi)/(v_c Q)\}$. Over the analyzed band (10–40 Hz), the exponential term is highly sensitive to $\xi$ and controls the shape of the high-frequency roll-off, whereas the power-law factor primarily modulates the spectral slope and governs the overall decrease in PSD magnitude as $\xi$ decreases.

To estimate $\xi$ for each surge, we numerically solve the following inversion equation:

$$P/P_0 = \mathcal{P}(\xi)/\mathcal{P}(\xi_0) \quad (4)$$

Equation 4 is inverted using the nonlinear root-finding algorithm fsolve from the SciPy library. The inversion was performed over the 10–40 Hz frequency band, with an initial guess of $\xi = 0.4$, a convergence tolerance of $10^{-4}$, and no additional parameter bounds applied. Following the formulation of Lai et al. (2018), $\xi$ describes the frequency dependence of Rayleigh-wave phase velocity and the associated structural control on frequency-dependent attenuation, rather than intrinsic energy dissipation (Tsai et al., 2012). We adopted a baseline value $\xi_0 = 0.4$ for the first surge, consistent with previous studies that reported $\xi \approx 0.25$–$0.5$ for firm, non-liquefied sediments (Lai et al., 2018). Subsequent $\xi$ values were obtained by fitting Equation 2) to the observed PSD decay and expressed relative to this reference ($\Delta\xi = \xi - \xi_0$). Variations in $\xi$ relative to the baseline value $\xi_0$ reflect changes in the near-surface velocity structure. A decrease in $\xi$ leads to stronger frequency-dependent exponential decay in the PSD formulation, reducing the effective transmission of high-frequency seismic energy to the station. This inversion is repeated for all surges ($i = 2, 3, \ldots, N$), yielding a surge-by-surge time series of $\xi$ values that isolate the evolving seismic damping behavior induced by inter-surge deposition layers.

While Equation 4 provides only an order-of-magnitude approximation, its relative formulation allows robust comparisons between surges recorded by the same sensor. This physically grounded inversion framework enables tracking of the dynamic channel-bed conditions during debris-flow sequences, and provides a mechanistic basis for interpreting variations in seismic signal amplitude.

Together, these two approaches provide complementary perspectives on debris-flow seismogenesis. The energy-scaling analysis treats the surge as an integrated mass, directly relating its bulk kinetic energy to the observed seismic amplitude. In contrast, the PSD-based model resolves seismic radiation as the theoretical superposition of individual particle–bed impacts, with the $\xi$ parameter capturing surge-to-surge changes in effective high-frequency transmission associated with evolving near-surface structure. Viewed jointly, the first approach highlights the macroscopic correspondence between flow energetics and ground motion, while the second offers a mechanistic framework for interpreting how evolving bed conditions modulate the seismic signal.

## 4. Results

### 4.1. Disrupted Seismic–Scale Relationship Due To Deposition Layers

To evaluate our hypothesis that evolving basal deposition layers modulate seismic transmission, we analyzed the surge-by-surge seismic and flow characteristics during the 28 July 2024 debris-flow event at Jiangjia Ravine. Specifically, we examined the relationship between individual surge size—characterized by flow thickness and velocity—and the corresponding seismic amplitude recorded by near-field geophones. The results were compared with previously published data from Gadria Creek (Coviello et al., 2019) to assess the influence of subsurface evolution on seismic response consistency.

As shown in Figure 7a, a generally positive linear relationship exists between the surge scale and peak seismic amplitude, in line with physical expectations that larger flows exert greater dynamic loading on the channel bed. This trend is qualitatively consistent with field data reported by Coviello et al. (2019), who observed a strong coupling between surge scale and seismic signal strength. However, quantitative comparison reveals a marked difference in fit quality: while Coviello et al. reported a high coefficient of determination ($R^2 = 0.833$), our data set yields only a moderate correlation ($R^2 = 0.443$).

To further investigate the discrepancy between seismic and dynamic metrics, we provide surge-by-surge supplementary analyses in Figures S2–S4 in Supporting Information S1. Figure S2 in Supporting Information S1 presents the evolution of debris-flow kinematic parameters, including front velocity and kinetic energy, showing that the dynamic intensity of the surges does not exhibit a systematic decline throughout the event. Figure S3 in Supporting Information S1 displays the corresponding seismic metrics—peak amplitude and Arias intensity—and reveals a progressive reduction in seismic energy in the later surges. Figure S4 in Supporting Information S1 compares these seismic parameters with normalized kinetic energy, demonstrating that while peak amplitude retains a moderate positive association with flow intensity, Arias intensity shows no clear correlation. Collectively, these Supporting Information S1 results confirm that the observed seismic dampening cannot be attributed solely to changes in surge magnitude or energy. Instead, they support our interpretation that the

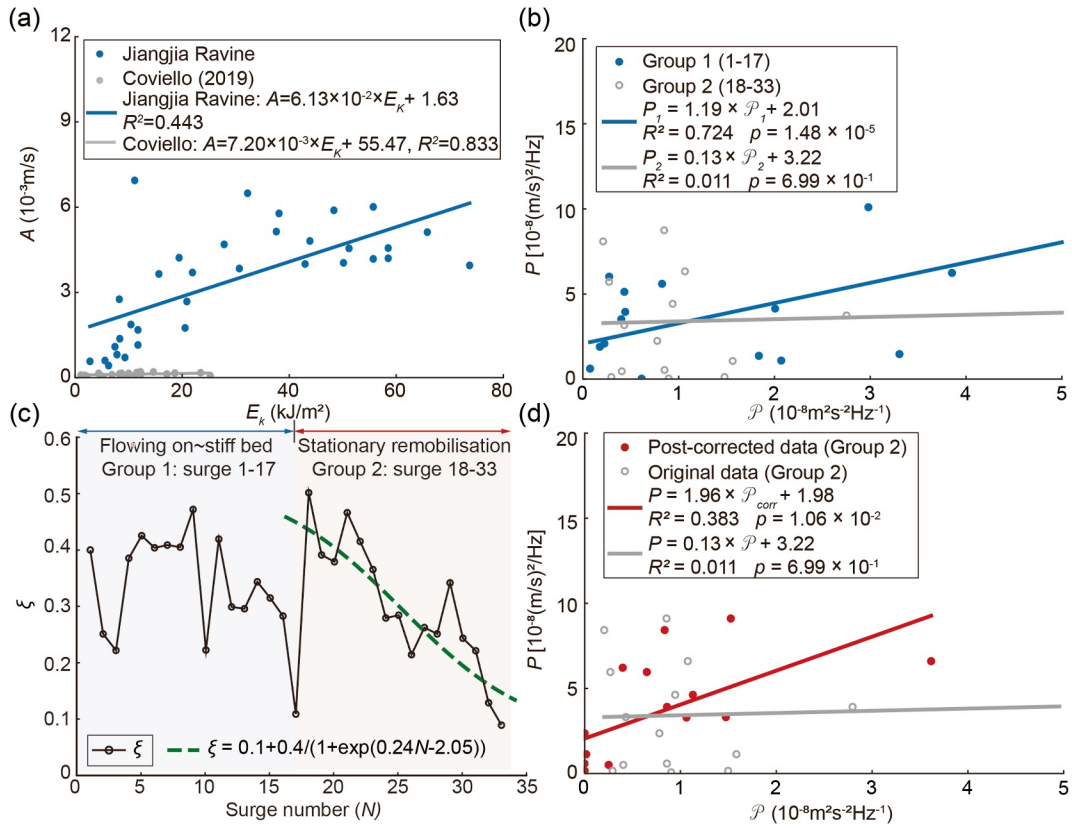


**Figure 7.** Influence of deposition layer on seismic signal attenuation. (a) Comparison of surge scale and seismic amplitude using our data (33 surges) and Coviello et al. (2019). (b) Modeled PSD versus observed seismic amplitude based on Lai et al. (2018). Group 1 (with intermittent continuous flow) shows strong linearity ($R^2 = 0.724$), while Group 2 (pure surges) shows poor fit ($R^2 = 0.011$), reflecting signal attenuation by buildup of deposition layer. (c) Inversion-derived $\xi$ values as a function of surge number ($N$) for the 28 July 2024 debris flow event at Jiangjia Ravine. The green dashed line represents the sigmoid function fitted to Group 2, capturing the progressive attenuation effect of evolving subsurface deposition layers. (d) Sigmoid empirical fit linking $\xi$ to surge number $N$, and improved seismic model performance after incorporating the deposition-dependent $\xi$ into the theoretical framework.

progressive evolution of the basal deposition layer exerts increasing control over seismic-wave propagation during the later stages of the event.

This discrepancy suggests that the surge–seismic amplitude relationship in Jiangjia Ravine is influenced by additional attenuating factors not prominent at Gadria Creek. We attribute this weaker correlation to the presence and progressive development of liquefied deposition layers between surges. As successive surges traverse an increasingly saturated and deformable substrate, energy transmission into the bedrock is likely dampened through mechanisms such as viscous dissipation in pore fluids, scattering by structural heterogeneity, and disruption of granular force chains. These processes introduce nonlinearity and variability into the seismic response, effectively decoupling seismic amplitude from surge size (Figures 2–5).

This interpretation is further supported by several anomalous surge comparisons. For instance, Surge 11 (03:30:50 UTC) generated a much stronger seismic response than Surge 27 (03:44:51 UTC), despite being smaller in scale (0.4 vs. 0.6 m in flow thickness). Such examples underscore the role of evolving bed conditions—rather than flow magnitude alone—in shaping ground vibration signals during debris-flow sequences.

### 4.2. Subsurface Evolution Decouple PSD–Energy Scaling in Surge-Type Flows

While the empirical framework proposed by Coviello et al. (2019) offers valuable insight into the scaling relationship between debris-flow magnitude and seismic amplitude, it largely neglects the mechanical evolution of the channel bed—particularly the role of dynamically accumulating deposition layers during multi-surge events.

Their model conceptualizes debris flows as uniform masses traveling over a static substrate, assuming direct energy coupling between surge momentum and ground vibration. However, such assumptions may not hold in field conditions where the subsurface evolves rapidly.

In contrast, the theoretical formulation by Lai et al. (2018) explicitly links seismic power spectral density (PSD) to particle–bed interactions and incorporates the influence of substrate mechanical properties. This enables us to assess how inter-surge deposition modulates seismic signal strength beyond surge size alone. By integrating both frameworks, we aim to capture the progressive decoupling of seismic energy transmission as the basal layers evolve.

As shown in Figure 4b, a distinct difference emerges between two surge groups. In Group 1 (surges 1–17), a strong linear relationship was observed between modeled PSD and measured seismic amplitude ($R^2 = 0.724$, $p < 0.005$), indicating robust coupling consistent with both Coviello's empirical and Lai's physical model assumptions. However, in Group 2 (surges 18–33), the correlation breaks down entirely ($R^2 = 0.011$), reflecting a near-total decoupling between modeled energy input and actual seismic output.

This deterioration aligns with our hypothesis that continuous flow in early stages helps prevent significant layer accumulation, thus maintaining a stable bed condition and effective seismic coupling. Once the continuous flow subsides and the inter-surge intervals lengthen, sediment progressively accumulates at the bed, creating deformable and energy-absorbing layers. These deposition layers likely absorb and scatter incoming energy, leading to non-linear damping and ultimately obscuring the expected PSD–seismic amplitude scaling.

To better quantify this evolving attenuation behavior, we invert $\xi$ as an effective near-surface transmission parameter within the Lai et al. (2018) PSD framework, $\xi$, from Lai et al. (2018). This dimensionless parameter captures the combined effect of substrate thickness, stiffness, and energy dissipation properties, providing a physically grounded measure of how deposition layers modulate seismic transmission over time. While the Lai model explains instantaneous variations between surges, the $\xi$ parameter enables us to track surge-by-surge changes in effective seismic transmission efficiency associated with evolving near-bed structure.

### 4.3. Attenuation Parameter $\xi$ Captures the Modulating Role of Evolving Deposition Layers

Building on the parameterization framework described above, we further investigate the relationship between the parameter $\xi$ and the thickness of the deposition layer. As shown in Figure 7c, during the sequence of surge-type debris flows, the $\xi$ values inverted from Equation 4 exhibit distinct temporal patterns across the two groups.

In the Group 1, which experiences intermittent continuous flow, $\xi$ values fluctuate—alternating between increases and decreases—consistent with our earlier hypothesis that continuous flow episodes erode or thin deposition layers, thereby reducing their attenuating effect. In contrast, the Group 2, characterized by purely discrete surges, shows a monotonic decline in $\xi$ over time. This trend suggests that as the number of surges increases, the deposition layer progressively accumulates and liquefies, increasingly damping seismic wave transmission. The $\xi$ values approach a lower asymptote near 0.1, consistent with a fully saturated and mechanically weakened subsurface (Zhang et al., 2021).

As shown in Figure 7c, $\xi$ values decrease systematically with the surge sequence, indicating a progressive reduction in the effective transmission of high-frequency seismic energy. This behavior arises from enhanced frequency-dependent exponential decay associated with changes in the near-surface velocity structure induced by the evolving liquefied deposition layer. This pattern supports our interpretation of $\xi$ as a proxy for the evolving mechanical influence of inter-surge deposition layers on seismic signal propagation.

To capture this relationship quantitatively, we propose an empirical fitting equation that links $\xi$ to surge number, reproducing the observed nonlinear attenuation trend. This relationship not only reflects the progressive energy damping induced by sediment accumulation but also serves as a generalizable tool for extending seismic-based interpretations of subsurface conditions to other debris-flow-prone environments. It provides a practical framework for inferring the time-evolving flow–bed interactions where direct measurements are unavailable.

The proposed empirical function is given by

$$\xi = 0.1 + \frac{0.4}{1 + e^{0.24N - 2.05}} \tag{5}$$

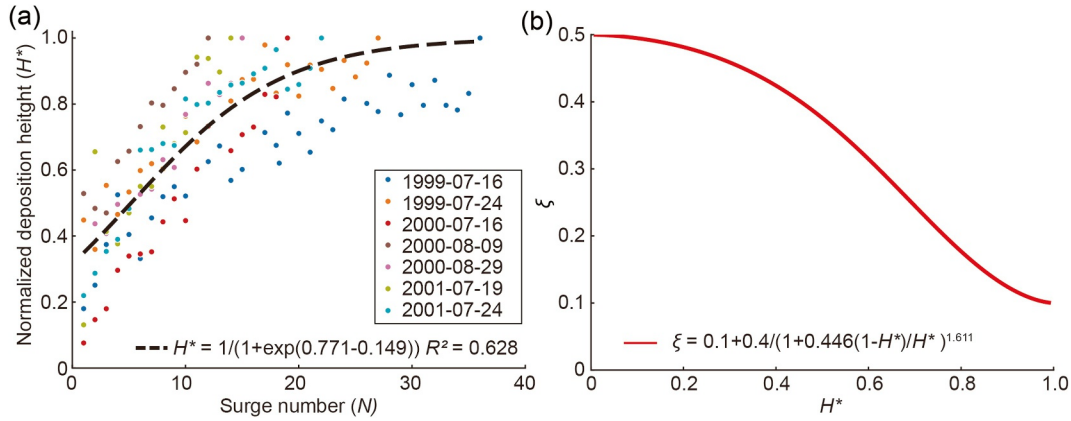


**Figure 8.** Influence of deposition layer on seismic wave attenuation. (a) Progressive increase in normalized deposition layer thickness ($H^*$) with surge number ($N$) across seven multi-surge debris flow events observed at Jiangjia Ravine from 1999 to 2001. The accumulation follows a logistic (sigmoid) growth pattern, characterized by rapid early-stage sediment buildup and subsequent saturation constrained by channel topography. (b) Inverse nonlinear relationship between the attenuation parameter ($\xi$) and normalized deposition layer thickness ($H^*$). As $H^*$ increases, $\xi$ decreases asymptotically, approaching a lower bound. This behavior indicates enhanced seismic damping as the liquefied basal layer thickens, suggesting that signal attenuation is strongly modulated by the evolving structure of the subsurface bed.

This sigmoid-shaped equation offers several advantages. It provides physically meaningful upper and lower bounds for $\xi$ (Tsai et al., 2012), corresponding respectively to early-stage minimal attenuation and late-stage saturated conditions. The decline rate and the inflection point—controlled by the exponential term—can be adjusted to reflect different channel morphologies or sediment dynamics, enhancing its site-specific applicability and potential for broader use in debris flow monitoring.

By incorporating this empirically calibrated $\xi$ value into Equation 2, we recalculated the seismic power spectral density $\mathcal{P}$ for each surge in Group 2. The resulting regression analysis shows a marked improvement in linearity, with the coefficient of determination ($R^2$) increasing from 0.011 to 0.383 and the $p$-value decreasing from 0.70 to 0.0106. This enhancement indicates that once the influence of the deposition layer is properly accounted for, the seismic response predicted by Lai's theoretical model aligns more closely with the observed data. These findings strongly support our hypothesis that the deposition layer significantly modulates seismic wave propagation and must be considered in physical modeling frameworks.

### 4.4. Attenuation Parameter $\xi$ Quantitatively Tracks Observed Deposition Layer Buildup

To further explore the physical meaning of $\xi$, we conducted a quantitative analysis linking $\xi$ to measured deposition layer thickness based on long-term field data from Jiangjia Ravine between 1999 and 2001. As an initial step, we examined the relationship between the number of surge events ($N$) and the residual deposition layer thickness ($H$, m), which was consistently measured after debris-flow sequences.

As shown in Figure 8a, the normalized deposition height $H^*$—computed as the measured deposition thickness normalized by its event-specific maximum value ($H/H\text{max}$)—exhibits a systematic and self-similar progression across seven independent debris-flow events from 1999 to 2001. Despite differences in magnitude and hydrologic forcing, all events display the same characteristic pattern: $H^*$ rises sharply during the early surges and then gradually approaches a saturation level.

Taken together, these independent lines of evidence—historical measurements and contemporary field observations—demonstrate that deposition height and surge number are strongly linked at Jiangjia Ravine. This validates the use of the 1999–2001 $H^*$ data (Chen & Song, 2023) as a physically robust analogue for interpreting basal-layer evolution during the 2024 event, even though direct thickness measurements were unavailable for 2024. The recurrence of a self-similar buildup curve across events supports the conclusion that basal-layer thickening is governed by intrinsic surge-sequence mechanics rather than by year-specific external conditions. As shown in Figure 8a, the normalized deposition height $H^*$, obtained by dividing the measured deposition thickness by its maximum value ($H/H_{max}$), increases systematically with the number of surges $N$ across multiple

debris flow events. Each colored dot represents an individual surge within a specific event, with data spanning seven separate debris flow events (1999-07-16 to 2001-07-24). Despite variability among events, all exhibit a consistent upward trend in $H^*$, indicating that deposition layers accumulate progressively during multi-surge sequences.

To quantitatively describe this relationship, we fit a logistic growth function:

$$H^* = \frac{1}{1 + e^{-0.149N+0.771}} \tag{6}$$

This sigmoid function (black dashed line in Figure 8a) captures the nonlinear accumulation pattern of deposition layers, with a relatively rapid initial increase followed by a gradual saturation as the surge number $N$ exceeds ~20.

This pattern reflects a physically intuitive process: early surges deposit material efficiently onto a relatively bare channel bed, whereas subsequent surges increasingly interact with pre-existing deposits, leading to reduced incremental deposition and an eventual asymptotic behavior. The logistic form also aligns with the expectation that topographic saturation and sediment mobilization capacity constrain the maximum achievable deposition thickness under gentle slope conditions (Edwards et al., 2021).

By combining the empirical relationships of $\xi$–$N$ and $H^*$–$N$, we further derived an explicit expression linking $\xi$ to normalized deposition layer thickness $H^*$:

$$\xi = 0.1 + \frac{0.4}{1 + 0.446\left(\frac{1-H^*}{H^*}\right)^{1.611}} \tag{7}$$

As shown in Figure 8b, the derived $\xi$–$H^*$ relationship exhibits a smooth nonlinear decline, consistent with theoretical expectations of increasing signal attenuation as deposition layers become thicker. When the normalized deposition layer height $H^*$ is low, $\xi$ remains high (approaching 0.5), indicating limited damping and efficient seismic transmission. However, as $H^*$ increases beyond 0.5, $\xi$ rapidly decreases and asymptotically approaches ~0.1. This pattern confirms the strong attenuation effect of well-developed liquefied subsurface layers and highlights the nonlinear nature of seismic damping in evolving sediment beds.

This monotonic inverse relationship highlights the critical role of deposition layer buildup in controlling seismic response. More importantly, it demonstrates that $\xi$—originally introduced as an effective transmission parameter—can now be physically linked to measurable sedimentary properties, providing a valuable parameterization for future seismic modeling and inversion of subsurface conditions during debris-flow sequences.

## 5. Discussion

Our findings point to a reframing of how seismic signals from debris-flow surges should be interpreted, particularly under multi-surge conditions. Field observations at Jiangjia Ravine document a pronounced *decoupling* between surge size and seismic amplitude as the flow sequence progresses. Contrary to the common assumption that larger surges generate stronger ground motion at fixed sensors (e.g., Coviello et al., 2019), our results consistently show that later larger surges often produce weaker seismic responses than earlier smaller ones. This discrepancy is most apparent during Group 2 of the 28 July 2024 event, where we observed stronger signals from thinner narrower surges early in the sequence compared to later larger surges (Figures 2–5).

This behavior is consistent with cyclic, surge-scale structural transitions described in the erosion–deposition wave (EDW) framework, which identifies alternating phases of basal arrest, temporary deposition, and remobilization in shallow granular flows (Edwards & Gray, 2015; Rocha et al., 2019; Takagi et al., 2011). Recent field observations confirm that EDW-like cycles occur within natural debris flows (Schöffl et al., 2023), and similar processes have been documented at Jiangjia Ravine (Chen et al., 2024).

We attribute this phenomenon to the progressive accumulation and liquefaction of inter-surge deposition layers, which alter the mechanical properties of the channel bed. As these deposition layers grow in thickness and lose structural integrity, they act as low-stiffness substrates that attenuate vertical ground motion. This interpretation is supported by both theoretical modeling and empirical evidence. Specifically, we extended the framework proposed by Lai et al. (2018) by introducing an attenuation parameter ($\xi$) to represent the influence of basal layering

on seismic wave transmission. The inclusion of $\xi$ in the model substantially enhances the fit between predicted and observed power spectral densities (Figure 7), thereby validating the role of evolving bed conditions in controlling seismic energy generation at the source. Although $\xi$ is not a dissipation parameter in a strict seismological sense, its decrease under progressively liquefied bed conditions leads to a reduction in the predicted seismic PSD through a lowering of the power-law exponent in the adopted formulation. While the exponential attenuation term becomes weaker as $\xi$ decreases, this effect provides only limited compensation and is outweighed by the dominant reduction in the power-law prefactor. Consequently, seismic amplitudes recorded at the station decrease even when flow dynamics remain comparable, explaining the observed decoupling between surge magnitude and seismic response during later stages of multi-surge debris-flow events.

In addition to modulating the generation of ground motion at the source, the evolving deposition layer affects the propagation of seismic waves near the surface. The accumulation of a soft water-rich substrate introduces enhanced scattering and impedance contrasts along the shallow propagation path, thereby reducing the effective transmission of high-frequency seismic energy. In our formulation, these surge-to-surge propagation effects are not interpreted as changes in the intrinsic quality factor $Q$, which is held fixed, but are instead captured in an effective sense by variations in the parameter $\xi$, which controls the frequency-dependent attenuation term in the PSD model. This treatment enables robust relative comparisons among surges recorded at the same station without requiring independent inversion of propagation parameters. In this sense, the basal layer acts not only as a mechanical buffer that weakens source coupling but also as an evolving near-surface filter that progressively suppresses high-frequency energy during wave propagation. Together, these effects provide a unified physical explanation for the observed surge-by-surge reduction in seismic amplitudes and spectral content.

Unlike previous studies that focused on pre-event or persistent surface deposits (e.g., Kean et al., 2015), our results highlight the importance of transient, dynamically formed deposition layers that arise during debris-flow activity and correspond to the basal-arrest phases described in EDW theory. These ephemeral beds are particularly prevalent in low-gradient channels where flow velocity periodically declines, enabling temporary sediment accumulation between surges. Such layers may be partially or entirely flushed post-event, leaving little surface trace yet exerting considerable influence during the event itself. Their cryptic nature has likely contributed to underappreciation in past seismic analyses.

This attenuation mechanism has direct implications for seismic-based debris-flow warning systems. Many existing systems rely on the assumption that larger surges reliably exceed a fixed detection threshold (Abancó et al., 2014; Badoux et al., 2009). However, our results suggest that even high-magnitude surges can yield weak seismic signatures if preceded by extensive deposition, potentially leading to underestimation of hazard intensity *or* missed detections during critical late-stage flows. Adaptive detection thresholds that account for evolving bed conditions—such as those inferred from $\xi$—may substantially improve monitoring accuracy.

Finally, the strong empirical relationship between $\xi$ and both surge number ($N$) and normalized deposition thickness ($H*$) (Figure 8) offers a practical inversion tool for inferring subsurface evolution. This is especially valuable in remote mountain settings where direct monitoring of bed material is infeasible. Such capability supports the future development of physics-informed seismic models that dynamically integrate subsurface state variables for real-time hazard interpretation.

## 6. Conclusions

This study demonstrates that inter-surge deposition layers, particularly when liquefied, exert a dominant control over ground motion generated by debris-flow surges. Analyses of multi-surge events at Jiangjia Ravine show that the progressive development of liquefied inter-surge deposition layers reduces seismic signals by weakening source–bed coupling and enhancing near-surface filtering of high-frequency energy during propagation. To quantify this effect, we introduce an effective transmission parameter ($\xi$) and incorporate it into an extended version of Lai et al.'s (2018) theoretical model, which substantially improves the predictive accuracy of seismic power spectra.

The empirical relationships among $\xi$, surge number $N$, and normalized deposition thickness ($H*$) provide a practical framework for non-invasive inversion of channel-bed state during debris-flow events. These results further indicate that seismic early-warning systems may benefit from adaptive, state-aware detection strategies; accounting for $\xi$-inferred bed evolution could reduce the risk of missed detections during late-stage surges.

## Inclusion in Global Research Statement

This research was led by the Institute of Mountain Hazards and Environment, Chinese Academy of Sciences, Chengdu, China. All individuals who meet the AGU Publications authorship criteria have been appropriately included as co-authors. The research adhered to the principles of equitable collaboration, including the co-development of research plans and shared access to data and outcomes among all partners.

## Conflict of Interest

The authors declare no conflicts of interest relevant to this study.

## Data Availability Statement

The field observation data of debris flows at Jiangjia Ravine were obtained from the Dongchuan Debris Flow Observation and Research Station (DDFORS) of Chinese Academy of Sciences. Seismic data of debris flow are available at https://doi.org/10.12072/ncdc.ddfors.db6804.2025 (Song et al., 2025b). The movie of the downward erosion of surge flows on 28 July 2024 at the Jiangjia Ravine is available at https://cstr.cn/CSTR:11738.11.NCDC.DDFORS.DB6807.2025 (Song et al., 2025c).

**Acknowledgments**
The authors acknowledge the financial supports from the National Natural Science Foundation of China (Grant 42477193) and National Cryosphere Desert Data Center (Grant E01Z790201). We would like to thank the Dongchuan Debris Flow Observation and Research Station (DDFORS) of the Chinese Academy of Sciences, which provides the field observation data of Jiangjia Ravine debris flows. Supported by the Science and Technology Research Program of Key Laboratory of Mountain Hazards and Engineering Resilience, Chinese Academy of Sciences (Grant KLMHER-TO6).

## References

Aaron, J., Spielmann, R., McArdell, B. W., & Graf, C. (2023). High-frequency 3D LiDAR measurements of a debris flow: A novel method to investigate the dynamics of full-scale events in the field. *Geophysical Research Letters*, *50*(5), e2022GL102373. https://doi.org/10.1029/2022GL102373

Abancó, C., Hürlimann, M., & Moya, J. (2014). Analysis of the ground vibration generated by debris flows and other torrential processes at the Rebaixader monitoring site (Central Pyrenees, Spain). *Natural Hazards and Earth System Sciences*, *14*(4), 929–943. https://doi.org/10.5194/nhess-14-929-2014

Bachelet, V., Mangeney, A., De Rosny, J., Toussaint, R., & Farin, M. (2018). Elastic wave generated by granular impact on rough and erodible surfaces. *Journal of Applied Physics*, *123*(4), 044901. https://doi.org/10.1063/1.5012979

Badoux, A., Graf, C., Rhyner, J., Kuntner, R., & McArdell, B. W. (2009). A debris-flow alarm system for the Alpine Illgraben catchment: Design and performance. *Natural Hazards*, *49*(3), 517–539. https://doi.org/10.1007/s11069-008-9303-x

Belli, G., Walter, F., McArdell, B., Gheri, D., & Marchetti, E. (2022). Infrasonic and seismic analysis of debris-flow events at Illgraben (Switzerland): Relating signal features to flow parameters and to the seismo-acoustic source mechanism. *Journal of Geophysical Research: Earth Surface*, *127*(6). https://doi.org/10.1029/2021JF006576

Berger, C., McArdell, B. W., & Schlunegger, F. (2011). Direct measurement of channel erosion by debris flows, Illgraben, Switzerland. *Journal of Geophysical Research*, *116*(F1). https://doi.org/10.1029/2010JF001722

Chen, Q., & Song, D. (2023). Flow depth measured by ultrasonic sensors and kinematic elements of surge flows in Jiangjia Ravine [Dataset]. *Dongchuan, Yunnan, China 1999-2001*. https://doi.org/10.12380/Debri.msdc.000012

Chen, Q., Song, D., Chen, X., Feng, L., Li, X., Zhao, W., & Zhang, Y. (2024). The erosion pattern and hidden momentum in debris-flow surges revealed by simple hydraulic jump equations. *Water Resources Research*, *60*(11), e2023WR036090. https://doi.org/10.1029/2023WR036090

Chen, Q., Song, D., Chen, X., & Zhong, W. (2023). Visco-collisional scaling law of flow resistance and its application in debris-flow mobility. *Journal of Geophysical Research: Earth Surface*, *128*(2), e2022JF006712. https://doi.org/10.1029/2022JF006712

Coe, J., Kean, J., McCoy, S., Staley, D., & Wasklewicz, T. (2010). Chalk Creek Valley: Colorado's natural debris-flow laboratory. In *Generations: Geologic and anthropogenic field excursions in the Rocky mountains from modern to ancient* (pp. 95–117). https://doi.org/10.1130/2010.0018(05)

Coviello, V., Arattano, M., Comiti, F., Macconi, P., & Marchi, L. (2019). Seismic characterization of debris flows: Insights into energy radiation and implications for warning. *Journal of Geophysical Research: Earth Surface*, *124*(6), 1440–1463. https://doi.org/10.1029/2018JF004683

Davies, T. R. H. (1986). Large debris flows: A macro-viscous phenomenon. *Acta Mechanica*, *63*(1), 161–178. https://doi.org/10.1007/BF01182546

Davies, T. R. H., Phillips, C., Pearce, A., & Zhang, X. (1992). *Debris flow behaviour– An integrated overview* (Vol. 209). IAHS Publication. Retrieved from https://iahs.info/uploads/dms/9009.217-225-209-Davies.pdf

Deparis, J., Jongmans, D., Cotton, F., Baillet, L., Thouvenot, F., & Hantz, D. (2008). Analysis of rock-fall and rock-fall avalanche seismograms in the French Alps. *Bulletin of the Seismological Society of America*, *98*(4), 1781–1796. https://doi.org/10.1785/0120070082

Edwards, A. N., & Gray, J. M. N. T. (2015). Erosion-deposition waves in shallow granular free-surface flows. *Journal of Fluid Mechanics*, *762*, 35–67. https://doi.org/10.1017/jfm.2014.643

Edwards, A. N., Viroulet, S., Johnson, C. G., & Gray, J. (2021). Erosion-deposition dynamics and long distance propagation of granular avalanches. *Journal of Fluid Mechanics*, *915*, A9. https://doi.org/10.1017/jfm.2021.34

Hibert, C., Mangeney, A., Grandjean, G., & Shapiro, N. M. (2011). Slope instabilities in Dolomieu crater, Réunion Island: From seismic signals to rockfall characteristics. *Journal of Geophysical Research*, *116*(F4), F04032. https://doi.org/10.1029/2011JF002038

Hu, W., Van Asch, T. W., Zheng, Y., Li, Y., Xu, Q., Huang, R., & McSaveney, M. (2022). Unraveling the effect of a two-layer system on the mobility of rapid gravitational flows. *Engineering Geology*, *297*, 106481. https://doi.org/10.1016/j.enggeo.2021.106481

Jiang, F., Dai, F., Zhou, J., & Jiang, R. (2023). AI-powered automatic detection of dynamic triggering of earthquake based on microseismic monitoring. *Soil Dynamics and Earthquake Engineering*, *165*, 107723. https://doi.org/10.1016/j.soildyn.2022.107723

Kean, J. W., Coe, J. A., Coviello, V., Smith, J. B., McCoy, S. W., & Arattano, M. (2015). Estimating rates of debris flow entrainment from ground vibrations. *Geophysical Research Letters*, *42*(15), 6365–6372. https://doi.org/10.1002/2015GL064811

Kean, J. W., McCoy, S. W., Tucker, G. E., Staley, D. M., & Coe, J. A. (2013). Runoff-generated debris flows: Observations and modeling of surge initiation, magnitude, and frequency. *Journal of Geophysical Research: Earth Surface*, *118*(4), 2190–2207. https://doi.org/10.1002/jgrf.20148

Lai, V. H., Tsai, V. C., Lamb, M. P., Ulizio, T. P., & Beer, A. R. (2018). The seismic signature of debris flows: Flow mechanics and early warning at Montecito, California. *Geophysical Research Letters*, *45*(11), 5528–5535. https://doi.org/10.1029/2018GL077683

Langham, J., Meng, X., Webb, J. P., Johnson, C. G., & Gray, J. M. N. T. (2025). Ill posedness in shallow multi-phase debris-flow models. *Journal of Fluid Mechanics*, *1015*, A52. https://doi.org/10.1017/jfm.2025.10297

Levy, C., Mangeney, A., Bonilla, F., Hibert, C., Calder, E. S., & Smith, P. J. (2015). Friction weakening in granular flows deduced from seismic records at the Soufrière Hills Volcano, Montserrat. *Journal of Geophysical Research: Solid Earth*, *120*(11), 7536–7557. https://doi.org/10.1002/2015JB012151

Li, A., Dai, F., Wu, W., Liu, Y., Liu, K., & Wang, K. (2022). Deformation characteristics of sidewall and anchorage mechanisms of prestressed cables in layered rock strata dipping steeply into the inner space of underground powerhouse cavern. *International Journal of Rock Mechanics and Mining Sciences*, *159*, 105234. https://doi.org/10.1016/j.ijrmms.2022.105234

Li, A., Liu, Y., Dai, F., Liu, K., & Wei, M. D. (2020). Continuum analysis of the structurally controlled displacements for large-scale underground caverns in bedded rock masses. *Tunnelling and Underground Space Technology*, *97*, 103288. https://doi.org/10.1016/j.tust.2020.103288

Li, J., Y, J. M., Bi, C., & Luo, D. F. (1983). The main features of the mudflow in Jiang-Jia Ravine. *Zeitschrift Fur Geomorphologie*, *27*(3), 325341. https://doi.org/10.1127/zfg/27/1983/325

Marchi, L., Arattano, M., & Deganutti, A. M. (2002). Ten years of debris-flow monitoring in the Moscardo Torrent (Italian Alps). *Geomorphology*, *46*(1–2), 1–17. https://doi.org/10.1016/s0169-555x(01)00162-3

McArdell, B. W., Bartelt, P., & Kowalski, J. (2007). Field observations of basal forces and fluid pore pressure in a debris flow. *Geophysical Research Letters*, *34*(7). https://doi.org/10.1029/2006GL029183

McCoy, S., Kean, J. W., Coe, J. A., Tucker, G., Staley, D. M., & Wasklewicz, T. (2012). Sediment entrainment by debris flows: In situ measurements from the headwaters of a steep catchment. *Journal of Geophysical Research*, *117*(F3). https://doi.org/10.1029/2011JF002278

Nagl, G., Hübl, J., & Kaitna, R. (2020). Velocity profiles and basal stresses in natural debris flows. *Earth Surface Processes and Landforms*, *45*(8), 1764–1776. https://doi.org/10.1002/esp.4844

Rocha, F., Johnson, C., & Gray, J. (2019). Self-channelisation and levee formation in monodisperse granular flows. *Journal of Fluid Mechanics*, *876*, 591–641. https://doi.org/10.1017/jfm.2019.518

Schöffl, T., McArdell, B., Koschuch, R., Schreiber, H., Graf, C., Hübl, J., & Kaitna, R. (2025). Flow resistance variability in debris flows: Evaluating equations, critical stress, and scaling from high-resolution field data. *Landslides*. https://doi.org/10.1007/s10346-025-02611-x

Schöffl, T., Nagl, G., Koschuch, R., Schreiber, H., Hübl, J., & Kaitna, R. (2023). A perspective of surge dynamics in natural debris flows through pulse-Doppler radar observations. *Journal of Geophysical Research: Earth Surface*, *128*, e2023JF007171. https://doi.org/10.1029/2023JF007171

Song, D., Chen, X., Sadeghi, H., Zhong, W., Hu, H., & Liu, W. (2023). Impact behavior of dense debris flows regulated by pore-pressure feedback. *Journal of Geophysical Research: Earth Surface*, *128*(12), e2023JF007074. https://doi.org/10.1029/2023JF007074

Song, D., Dai, F., Liu, Y., Tan, H., & Wei, M. (2025a). An efficiently designed CNN-Transformer fusion network for automatic and real-time microseismic signal classification. *Tunnelling and Underground Space Technology*, *161*, 106534. https://doi.org/10.1016/j.tust.2025.106534

Song, D., Zhong, W., Li, X., & Wei, L. (2025b). Seismic data of debris flow at Jiangjia Ravine, Yunnan, China, from 2023 to 2024 [Dataset]. *National Cryosphere Desert Data Center*. https://doi.org/10.12072/ncdc.ddfors.db6804.2025

Song, D., Zhong, W., Li, X., & Wei, L. (2025c). Video of debris flows that occurred in 2023 and 2024 at Jiangjia Ravine, Dongchuan, Yunnan, China [Dataset]. *National Cryosphere Desert Data Center*. https://doi.org/10.12072/ncdc.ddfors.db6807.2025

Takagi, D., McElwaine, J. N., & Huppert, H. E. (2011). Shallow granular flows. *Physical Review E*, *83*(3), 031306. https://doi.org/10.1103/PhysRevE.83.031306

Tsai, V. C., Minchew, B., Lamb, M. P., & Ampuero, J. P. (2012). A physical model for seismic noise generation from sediment transport in rivers. *Geophysical Research Letters*, *39*(2). https://doi.org/10.1029/2011GL050255

Viroulet, S., Edwards, A. N., Johnson, C. G., Kokelaar, B. P., & Gray, J. M. N. T. (2019). Shedding dynamics and mass exchange by dry granular waves flowing over erodible beds. *Earth and Planetary Science Letters*, *523*, 115700. https://doi.org/10.1016/j.epsl.2019.07.003

Wei, L., Song, D., Cui, P., Su, L., Zhou, G. G. D., Hu, K., et al. (2025). A long-term dataset of debris-flow and hydrometeorological observations from 1961 to 2024 at Jiangjia Ravine, China. *Earth System Science Data*. https://doi.org/10.5194/essd-2025-190

Zanuttigh, B., & Lamberti, A. (2007). Instability and surge development in debris flows. *Reviews of Geophysics*, *45*(3). https://doi.org/10.1029/2005rg000175

Zhang, J., Wu, J. S., You, Y., & Cheng, Z. L. (2003). Formation of residue layer of debris flow and the reduction of resistance. *Journal of Mountain Science*, *2*, 223–227. https://doi.org/10.16089/j.cnki.1008-2786.000601

Zhang, Z., Walter, F., McArdell, B. W., de Haas, T., Wenner, M., Chmiel, M., & He, S. (2021). Analyzing bulk flow characteristics of debris flows using their high frequency seismic signature. *Journal of Geophysical Research: Solid Earth*, *126*(12), e2021JB022755. https://doi.org/10.1029/2021JB022755

Zhou, Q., Tang, H., Hibert, C., Chmiel, M., Walter, F., Dietze, M., & Turowski, J. M. (2025). Enhancing debris flow warning via machine learning feature reduction and model selection. *Journal of Geophysical Research: Earth Surface*, *130*(4), e2024JF008094. https://doi.org/10.1029/2024JF008094

Zhou, Q., Tang, H., Turowski, J. M., Braun, J., Dietze, M., Walter, F., & Lagarde, S. (2024). Benford's law as debris flow detector in seismic signals. *Journal of Geophysical Research: Earth Surface*, *129*(9), e2024JF007691. https://doi.org/10.1029/2024JF007691

Zhou, X., Cui, Y., Fang, J., Tang, H., Zhang, Z., & Wang, S. (2025). Link between the impact mechanisms of granular flow-dam interaction and the generated seismic signal: Insights from laboratory experiments. *Journal of Geophysical Research: Solid Earth*, *130*(4), e2024JB029946. https://doi.org/10.1029/2024JB029946